NACA

RESEARCH MEMORANDUM

INVESTIGATION OF TWO-STAGE COUNTERROTATING COMPRESSOR I - DESIGN AND OVER-ALL PERFORMANCE OF TRANSONIC FIRST COMPRESSOR STAGE

By Ward W. Wilcox and Linwood C. Wright

Lewis Flight Propulsion Laboratory
Cleveland, Ohio

NATIONAL ADVISORY COMMITTEE
FOR AERONAUTICS

WASHINGTON

May 22, 1956

NACA RM E56C15

NATIONAL ADVISORY COMMITTEE FOR AERONAUTICS

RESEARCH MEMORANDUM

INVESTIGATION OF TWO-STAGE COUNTERROTATING COMPRESSOR

I - DESIGN AND OVER-ALL PERFORMANCE OF TRANSONIC FIRST COMPRESSOR STAGE

By Ward W. Wilcox and Linwood C. Wright

SUMMARY

A highly loaded transonic rotor was designed, built, and tested as part of a two-stage counterrotating-compressor research program. The design conditions, which were also chosen to explore the upper limits of loading and Mach number for the transonic unit, specified a pressure ratio of 2.03, a weight flow of 29.2 pounds per second per square foot of frontal area, and an adiabatic efficiency of 0.92. At the design-speed peak-efficiency point, a pressure ratio of 2.0 was obtained at a weight flow of 29.2 pounds per second per square foot of frontal area and an adiabatic efficiency of 0.87.

The discrepancies between the design and experimental results are analyzed on an over-all basis and from a spanwise variation of flow conditions. This rotor seemed suitable for the first stage of the counterrotating compressor; its use as a first-stage rotor in a conventional transonic compressor is also discussed. The range of operation at each speed is comparable with that obtained with rotors having lower loading.

The complete rotor design procedure is presented, in addition to the recorded stall traces and the techniques for obtaining such data.

INTRODUCTION

As a means of achieving the maximum compression in the fewest number of stages, counterrotation of succeeding rotors has been suggested for many years. The potentiality of this type of compressor has been investigated analytically on a one-dimensional basis in reference 1. Although practical mechanical considerations of a high-speed unit limit the number of counterrotating stages to two, the total-pressure ratio available from two stages was insufficient to fulfill cycle pressure-ratio requirements for conventional jet engines until the advent of transonic and supersonic

compressor stages. A supersonic compressor (e.g., ref. 2) characteristically has high tip speed, which imposes serious problems on the turbine design (as in ref. 3). On the other hand, counterrotation allows high work loading on the second stage of a compressor without the extremely high tip speeds.

The first stage of a counterrotating compressor derives no direct benefit from counterrotation except that stator limitations do not restrict the design. Because the stators are eliminated in this application, it may be possible to load the first-stage rotor more heavily than conventional rotors without exceeding the blade-element loading parameters commonly employed (ref. 4). In the particular rotor discussed in this report, the tip-section loading was carried beyond normal transonic-stage limits as part of a general study to determine the limits to which loading and Mach number could be extended. In this case, it was considered that, if necessary, the tip section could be unloaded by relatively simple modifications, whereas the opposite effect would be difficult to achieve.

In the design of this counterrotating compressor, which consists primarily of a highly loaded transonic rotor followed by a supersonic rotor, the experience from the rotors of references 5 to 8 was used. A major consideration was to keep the second-stage outlet Mach number at a low level to minimize the supersonic stator problems discussed in reference 9.

Whereas design-speed compressor performance may be calculated in a conventional manner, the performance at off-design speeds and at combinations of rotor speed was considered to be beyond analytical determination. To facilitate compressor and turbine matching studies from which engine pumping characteristics can be determined, it is necessary to have complete performance maps of both the compressor and the turbine. Preliminary analytical studies of counterrotating turbines that produce such maps are given in reference 10. One of the primary objectives of the counterrotating compressor program is to provide these maps for the compressor components.

In this report, the design, the over-all performance, and the stall characteristics of the first highly loaded transonic rotor are presented. In addition to its function as the first stage of the counterrotating compressor, this rotor was designed as a unit in which the performance of conventional blading could be evaluated at unconventional levels of loading and Mach number.

ROTOR DESIGN

General Considerations

In designing a compressor, it is usually necessary to go through preliminary calculations in order to establish the initial limits and critical problems of the design. For the two-stage counterrotating-compressor design, an over-all pressure ratio of 5 and a corrected specific weight flow of about 30 pounds per second per square foot of frontal area were desired. The work split was chosen so that the energy addition in the second stage was twice that in the first stage. The consideration of power available, gearing, and air services limited the nominal outer diameter to 16 inches.

Because of the high pressure ratio, the high weight flow, and the relatively short axial length desired for the first stage, it was necessary to estimate the effect of wall curvatures on the velocity distributions before and after the rotor. In order to minimize the effect of wall curvature on these velocity distributions, an arbitrary limit of 20° was set for the hub cone angle. This necessitated a reduction in the outer rotor tip diameter, which was defined by an analytical expression to ensure a smooth contour. In addition, it was considered necessary to employ an estimated radial variation of loss at the rotor outlet in order to define rotor-outlet conditions more exactly.

Other arbitrary specifications for the first-stage rotor were as follows:

Nominal equivalent tip speed, $U_t/\sqrt{\theta_1}$, ft/sec	1260
Inlet hub-tip radius ratio, r_h/r_t	0.5
Design specific weight flow allowing a blockage factor of 0.98, lb/(sec)(sq ft)	30.6
Radially constant energy addition, Btu/lb	30.5
Rotor axial depth, in.	2.5
Chord length, in.	2.75
Hub cone angle	not over 20°

The tip speed of the transonic first-stage rotor corresponded to that of the rotor of reference 8 at 90 percent of design speed. The radial distribution of entropy determined in tests of the rotor (ref. 8) at 90-percent design speed was used as the predicted loss variation for the subject rotor. However, the rotor of reference 8 differed from the current rotor because it was not designed for radially constant energy addition and had an inlet hub-tip radius ratio of 0.7 instead of 0.5. Because of these dissimilarities, the resulting over-all pressure ratio and efficiency were slightly different from those of reference 8, the final computed values being 2.03 and 0.92, respectively.

[redacted]

Rotor-Inlet Conditions

Because of the time required for the more elaborate procedures (such as stream-filament methods), the following approximate procedure was adopted for the inlet-annulus design and estimation of the resulting axial velocity distribution. The rotor tip contour is given as a function of axial position by the following expression:

$$r_t = 8.000 - 0.0438z^3 + 0.0146z^4 - 0.0013z^5 \qquad (1)$$

where z equals the axial distance in inches from a fixed origin (axially, 1.0 in. upstream of the rotor blade leading edge at the hub).

The radius of curvature $r_{\mathscr{C}}$ of the outer wall at the compressor face (in the radial-axial plane) was 8.8 inches. At the inside wall, the bearing housing limited the minimum hub radius ratio to 0.4. In the radial-axial plane, a circular arc having a 9.25-inch radius was, therefore, drawn tangent to the 19° hub slope at the hub-tip radius ratio of 0.5 (rotor inlet) and tangent to the hub-tip radius ratio of 0.4 at zero slope (upstream of the rotor inlet).

The curvatures of the outer and the inner wall in the radial-axial plane were almost equal in magnitude but in opposite directions. At intermediate radii, a linear variation between the wall values was assumed, for simplicity. The velocity profile far upstream was assumed to be uniform. It was then assumed that the static-pressure gradient along the compressor-inlet radius r would be a function of the curvature in the radial-axial plane $1/r_{\mathscr{C}}$. For isentropic flow, this assumption appears to be a reasonable approximation for the conditions when the direction of the radii of curvature $r_{\mathscr{C},t}$ and $r_{\mathscr{C},h}$ and the compressor radius r are in the same direction. Under these assumptions, using the Bernoulli equation and the equation of motion, the following expression for the ratio of the velocity at any radius to the tip velocity was derived:

$$\frac{V}{V_t} = e^{-\left[m(r_t-r) - n(r_t^2-r^2)\right]} \qquad (2)$$

where the curvature was assumed to be fixed by the expression $1/r_{\mathscr{C}} = m + nr$, and the coefficients m and n were determined from the fixed hub and tip wall curvatures in the radial-axial plane. For this configuration, $m = 0.3310$ and $n = 0.02783$. (All symbols are defined in appendix A.)

A value of tip velocity V_t was chosen, and V was found at a number of radii. The weight flow was found by integrating ρV across the

[redacted]

annulus. If the integrated weight flow did not check the design value, the assumed V_t was altered and a new weight flow was obtained. This process was repeated until the desired weight flow resulted.

Rotor-Outlet Conditions

Because of the steep rotor hub, it was evident that the hub profile computations had to be carried through the interrotor space in order to determine the resulting change in flow conditions from the outlet of the first stage to the inlet of the second stage. For this reason, an interrotor calculation was set up to cover an axial distance greater than the expected interrotor spacing (fig. 1). This calculation (appendix B) begins with an assumed variation of axial velocity along the outer wall and considers radially constant energy addition, continuity, and a radial-equilibrium equation that neglects only the tangential variations for perfect fluid. From this procedure at any axial position, the variations of all flow parameters and of the radius were determined as functions of percent weight flow beginning with zero at the outer wall. The computations were terminated at the 100-percent-weight-flow radius when the hub radius and angle ε at the rotor outlet corresponded with the desired values. Cones generated by revolving the lines in the radial-axial plane connecting points of equal weight flow at the rotor inlet and outlet were defined as stream surfaces for blade layout purposes (fig. 1). The design results are compared with the experimental results in the subsequent data presentation figures.

Blade-Section Selection for Computed Velocity Diagrams

When the desired diagrams of first-stage rotor-inlet and -outlet velocities were determined, a physical blade still had to be prescribed that would produce the computed flow conditions. For the first-stage rotor, which is a high-performance transonic rotor, the conventional blade-element approach was used. Airfoil sections of double-circular-arc configuration having 4.5-percent-chord thickness at the tip and 9-percent-chord thickness at the hub were chosen for a constant 2.75-inch chord on the stream surfaces. Leading- and trailing-edge radii of 0.015 inch were specified. After surveying the optimum-incidence-angle data of several transonic rotors, an incidence angle of 5° at all radii was chosen. The deviation angle was estimated according to Carter's rule (ref. 11). The number of blades was determined as 22 for the nominal tip solidity of 1.2 and the 16-inch diameter.

Radii of an equal percent of weight flow at the rotor inlet and outlet (0, 20, 40, 60, 80, and 100 percent) were joined by straight lines, which were revolved about the axis to form conical surfaces (as shown in fig. 1). In order to maintain the desired rate of change in β along

the streamline, the double-circular-arc airfoil section was wrapped about these cones at the proper setting angle. For each conical blade element, the center of gravity was determined and the element centers of gravity were stacked on a radial line to form a blade. The blade inlet and outlet flow angles for the true circular-arc blade sections on the conical surfaces, as well as the inlet and outlet radii, are given in table I. The air is turned to much less than axial at the tip and beyond axial at the hub. The photograph of figure 2(a) shows the completed first-stage rotor.

APPARATUS AND PROCEDURE

Compressor Installation

In order to test the counterrotating compressor without the complication of coaxial shafts, two cantilever-type test rigs were placed face to face, each rig with its own variable-frequency motor and gearbox having a ratio of 5.521. A schematic sketch of the test rig with the first-stage rotor installed is given in figure 2(b). At the inlet, it was necessary to omit the usual depression tank; instead, the air was ducted around the first-stage motor, then through four inlets into an annular chamber. A honeycomb flow straightener was installed in this chamber to eliminate any tangential velocity components resulting from the four inlet pipes. The outlet throttles were placed at the two collector outlet pipes as near the collector exit as possible in order to prevent the volume between the rotor and the outlet valves from becoming excessively large.

The instrument stations are shown in figure 2(b). At station 0, fixed rakes were used to measure total pressure, static pressure, and total temperature at three circumferential and at five radial positions. In front of the first-stage rotor, station 1 (approx. 1 in. upstream of the rotor), radial surveys of total pressure, flow angle, and static pressure were made. Station 2, which was approximately 3/8 inch downstream of the rotor, was used for rating the performance of the first-stage rotor. At this station, radial surveys of total pressure, static pressure, flow angle, and total temperature were made. A fairing piece was installed in the position to be occupied by the second rotor; therefore, the inner wall curvature behind the rotor differed slightly from that existing when the second rotor was used. Numerous static wall taps were placed at various locations along the flow path on both the inner and outer walls. An adjustable orifice in the piping system was used to measure the weight flow.

The occurrence and frequency of rotating-stall pulses were determined with both hot-wire anemometers and pressure transducers connected to suitable electronic equipment. A complete description of the transducer apparatus, including a diagram showing bridge construction, hookup, and a description of the probe used, is included in appendix C.

Operating Procedure

After the motor speed necessary to establish the equivalent tip speed was set according to inlet temperature, a test point was obtained with the outlet throttles wide open (discharge air was ducted to laboratory exhaust system). Other test points were obtained by progressively closing the throttle position (at constant inlet pressure) until the condition of surge was reached.

Calculation Procedure

All measurements of pressure, temperature, and flow angle were corrected for Mach number, wire calibration, and so forth, according to instrument calibrations obtained in a separate wind tunnel. The computation of actual loss, loading, and over-all performance parameters was made according to the equations presented in appendixes A and B of reference 7.

RESULTS AND DISCUSSION

Over-All Performance

The over-all performance of the first-stage rotor is given in figure 3. In figure 3(a), the mass-weighted average total-pressure ratio is presented as a function of the specific weight flow (sea-level equivalent weight flow per unit frontal area). The range of equivalent speeds was varied from 50 to 110 percent of the design value of 1260 feet per second. From figure 3(a), it is evident that this rotor has conventional characteristic curves with an operating range at design speed comparable to rotors of lower levels of pressure ratio and inlet Mach number.

At design speed, the maximum weight flow attained was 30.3 pounds per second per square foot. The peak pressure ratio obtained at design speed was 2.0 as compared with the design value of 2.03. The highest weight flow at which rotating stall existed is indicated by the initial stall line. At low speeds, it was possible to obtain test points at lower weight flows to the stall-limit line. At higher speeds, the stall pulses were stronger and no determined effort was made to operate far into the stall region. Surge established the lower weight-flow limit at 100 and 110 percent of design speed.

The adiabatic efficiency of the first-stage rotor is plotted against specific weight flow in figure 3(b) for equivalent tip speeds of 50 to 110 percent of design. Peak efficiencies remain above 0.90 to a speed of 90 percent of design. However, peak efficiency drops off rapidly at 100- and 110-percent-design speeds. At design speed, the peak adiabatic

efficiency of 0.87 occurs at a specific weight flow of 29.2 pounds per second per square foot. A comparison of the actual blade angles with the analytical design values revealed an unaccountable error of +1.75° in blade-setting angle. An estimate of the weight flow corresponding to the design incidence angle at the actual blade-setting angles gives 29.2 pounds per second per square foot, which agrees with the peak-efficiency operating point.

In order to illustrate the average rotor-outlet conditions, mass-weighted average values of outlet flow angle and Mach number are given in figures 3(c) and (d), respectively. In figure 3(c), the average rotor-outlet flow angle is given as a function of the specific weight flow. At peak-efficiency weight flow and design speed, the average flow angle was about 46.5°. The mass-weighted average outlet Mach number $\overline{M_2}$ is given in figure 3(d) as a function of specific weight flow. At all speeds, the general Mach number level is high (lowest average Mach number, about 0.95 at design speed).

Although the over-all performance of this rotor suggests its use as the first stage of a conventional axial-flow compressor, high Mach number stators would be required to complete the stage. At all speeds above 80 percent of design, a stator cascade would operate in the transonic flow region. Present knowledge of stator design for this flow region and degree of turning is limited; and, to date, very little is known about transonic-stator performance. A counterrotating second-stage rotor would largely eliminate this problem by eliminating the need for interstage stators.

Design-Speed Performance

Outer-wall static-pressure distribution. - In figure 4, the static-pressure profiles over the rotor and part of the annulus are shown as the ratio of wall static pressure to inlet total pressure. Because each of the pressures shown is a time-average of the circumferential variation of static pressure, and the shock waves are skewed at an angle other than 90° with respect to the axis of rotation, conjecture is necessary to interpret the significance of the profiles. However, it is reasonably certain that the mode of operation within the rotor tip elements can be approximated. Four test points are given which cover the range of design-speed operating conditions. The specific weight flows for these points are

(1) Open throttle or minimum back pressure, choke flow;
$w\sqrt{\theta}/\delta A_F = 30.3$

(2) Maximum back pressure on vertical characteristics;
$w\sqrt{\theta}/\delta A_F = 30.0$

[redacted]

(3) Maximum efficiency; $w\sqrt{\theta}/\delta A_F = 29.2$

(4) Minimum-weight-flow, incipient-surge point; $w\sqrt{\theta}/\delta A_F = 27.4$

On any single blade element of this rotor, the minimum aerodynamic area is at the "closure line;" that is, at that normal from the suction surface of one blade which intersects the leading edge of the adjacent blade. This condition is typical of double-circular-arc airfoils at high stagger angles. In the radial-axial plane, however, the end walls are converging at an average 9° cone angle at the tip and a 19° cone angle at the hub. At the tip, the closure line intersects the suction surface downstream of the 50-percent-chord point because of the low solidity and high stagger angle. At the hub, where the solidity is much higher and the stagger angle is lower, the closure line intersects the blade suction surface at about 20-percent chord. Thus, the minimum three-dimensional area or throat consists of a curved surface nearer the blade inlet, and the aerodynamic area diverges downstream of this surface.

Figure 4 shows that, for the open-throttle point (30.3 lb/(sec)(sq ft)), the flow expands to supersonic velocities continuously downstream of the leading edge and then appears to go through some shock configuration just downstream of the passage inlet. This situation is analogous to flow in a Laval nozzle where the back pressure is low enough to attain sonic flow at the throat but too high for complete supersonic expansion throughout the diverging part of the nozzle. Despite this shock configuration, the computed relative Mach number is slightly supersonic at the trailing edge.

As back pressure is applied by throttling the outlet, the shock configuration moves forward in the diverging passage without changing the inlet conditions. Any number of points may be obtained on the vertical characteristic curve with corresponding tip wall pressure profiles between the 30.3 and 30.0 curves in figure 4. At the 30.0 point, virtually on the vertical operating curve, the shock configuration appears to move forward to take a position just forward of the closure line. Behind this shock, the flow is subsonic; and, with the diverging area, considerable subsonic diffusion takes place.

At the peak-efficiency point (29.2 lb/(sec)(sq ft)), the flow incidence angle is somewhat higher, resulting in greater expansion around the suction surface and a higher Mach number at the shock. In addition, the shock location seems to be moved forward slightly by the increased back pressure, resulting in a steeper static-pressure profile behind the leading edge. The losses near the tip are not decreased for this operating condition, but the peak efficiency is determined by the reduced losses at lower radii.

As back pressure is increased up to the incipient-surge point (weight flow, 27.4 lb/(sec)(sq ft)), the incidence angle increases and the shock position seems to move farther forward, resulting in a steeper tip wall pressure gradient. There is, in addition, inconclusive evidence (in the tip and hub wall static pressures) that a small amount of flow redistribution occurred upstream of the rotor inlet at high back pressures.

Radial variation of performance parameters. - Although the over-all performance of this rotor was generally satisfactory, the effect of the high level of Mach number and loading and the merit of the design procedure can be surmised only from examination of the radial variation of performance and flow parameters. In figure 5, the radial variations of pressure ratio, energy addition, and adiabatic efficiency are given for the four previously mentioned weight flows covering the weight-flow range.

The radial variation of pressure ratio is given in figure 5(a). At maximum flow with minimum back pressure, the pressure ratio is very low at the tip, but above design near the hub. However, the energy addition (fig. 5(b)) shows a similar trend; and, as a result, not all the decrease in pressure ratio (below the peak values) is derived from losses. The dashed lines, representing original design conditions, do not account for the 1.75° blade-setting error.

The wide radial variation in energy addition results from less-than-axial turning at the tip and beyond-axial turning at the hub. For turning the relative flow to the less-than-axial direction, relative velocities above design result in lower energy addition, while the opposite effect holds true for beyond-axial turning. Losses are high all across the span, as shown by the adiabatic efficiency (fig. 5(c)).

As back pressure is increased at the choke weight flow (30.0 lb/(sec)(sq ft)), the outlet relative velocity decreases and the energy addition shifts to a more uniform radial profile (fig. 5). Pressure ratio is increased at all radii except toward the hub where energy addition is reduced, and adiabatic efficiency is improved throughout. As discussed previously, further increase in back pressure decreases the weight flow and, thus, alters the inlet flow conditions. At the peak-efficiency weight flow of 29.2 pounds per second per square foot, the energy addition is relatively uniform radially and near design except for an increase near the tip. Losses near the tip are greater than anticipated, thus resulting in lower pressure ratios and adiabatic efficiencies than design. Near the hub, both pressure ratio and efficiency approach design values. At minimum weight flow, there is a further increase in energy addition at the outer radius, which results in a slightly higher pressure ratio and about the same efficiency in this region. At the hub, energy addition is the same as for peak efficiency, but the pressure ratio and efficiency drop because of increased losses.

Radial variation of inlet and outlet flow conditions. - The radial variation of inlet and outlet relative and absolute Mach numbers is given in figure 6 for the four design-speed test points just discussed. The inlet absolute Mach number (fig. 6(c)) shows a profile that varies somewhat from the original design. This profile demonstrates that the approximate method of computing the inlet flow distribution was not completely adequate. The measuring station was approximately 1 inch upstream of the rotor leading edge. In addition, one of the assumptions was that a uniform flow existed upstream of the region where rotor curvature effects apply. In this installation, with the radial inlet and sharp bend, it is doubtful that uniform flow could be expected. In fact, the velocity profile measured at station 0 was parallel to that observed at station 1. As a result of the velocity profile shown, the blade incidence angles were mismatched radially, so that it was impossible to operate at design incidence at all radii simultaneously.

The inlet Mach numbers relative to the blade are presented in figure 6(a). The slight variation from design shown is the result of the altered axial Mach number profile and the error in blade-setting angle. The variation from design is not considered serious and is generally less than the difference due to operating over a range of weight flows.

The outlet relative Mach number (in fig. 6(b)) demonstrates the two regions of flow within the blade. At open throttle, the outlet relative flow is entirely supersonic; at higher back pressures, the relative flow is subsonic. At maximum efficiency, the average outlet relative Mach number is close to the design value. The absolute outlet Mach numbers (fig. 6(d)) follow directly from vector addition of the relative values and the wheel speed. At open throttle, the absolute Mach number reaches very high values. At peak efficiency, the radial variation shows subsonic values at the outer radii and supersonic values at the inner radii, all within the transonic range.

The radial variation of outlet flow angle is given in figure 7(a) for design speed and the four representative weight-flow points. At choke flow and open throttle, the angles are low, but when the back pressure is applied and the relative Mach numbers (fig. 6(b)) approximate design, the outlet flow angles also approximate design. As pointed out earlier, these angles are rather high for turning back to the axial direction in a single blade row, as would generally be required for conventional compressor use.

As used in this counterrotating installation, the first-stage rotor is required not only to put out design pressure ratio and weight flow but also to set up the desired prerotation for the second stage. In figure 7(b), the radial variation of the tangential component of outlet velocity is shown. Over most of the useful weight-flow range, the outlet conditions for this rotor are sufficiently close to design for use with the second-stage rotor of the counterrotating compressor. However, the effect of the large tip losses on the second-rotor performance is obviously detrimental.

Suitability as First Stage of Conventional Axial-Flow Compressor

As mentioned previously, at rotor tip speeds above 80 percent of design, the outlet flow conditions would require the use of high-turning transonic stators in order to complete the stage. However, the performance at 80-percent speed (1008 ft/sec) may have interest for many compressor applications, inasmuch as a pressure ratio of 1.56 was obtained at a rotor adiabatic efficiency of 0.95 and a specific weight flow of 26.6 pounds per second per square foot. At this point, the average outlet flow angle was 39° and the average outlet Mach number was 0.85.

The radial variation of total-pressure ratio, energy addition, flow angle, and adiabatic efficiency are given in figure 8. At the maximum flow of 28.1 pounds per second per square foot, the uneven radial distribution of energy addition (fig. 8(b)) is the same as at design speed. Pressure ratio is low near the tip and higher near the hub (fig. 8(a)). Adiabatic efficiency peaks in midchannel, but is lower near the walls (fig. 8(d)). At the lower weight flows, energy addition is quite uniform radially and pressure ratio drops off less rapidly near the tip. Adiabatic efficiency is poor near the tip, but very good at other radii. Flow angles vary considerably with weight flow, but have a reasonably small variation in the radial direction (fig. 8(c)).

The radial variation of inlet and outlet relative and absolute Mach numbers is given in figure 9. Compared with design speed, the values of Mach number and the deceleration rates indicated are much lower; and, as a result, efficiency is better.

Stall Characteristics

Although the first-stage rotor was more ruggedly constructed than the usual production-model compressor rotor, the stall characteristics were determined in order to locate possible vibration problems. The particular blades used had a natural frequency much higher than most first-stage blades because of the high camber angle and the steep hub profile, so less trouble with harmonic vibrations was anticipated. It is possible, however, for a multiple-stall-zone flow to set up harmonic vibrations with a blade of high natural frequency.

As shown by the initial stall line on the characteristic map (fig. 3(a)), the first-stage rotor enjoyed a considerable stall-free range. At low speeds, it was possible to operate in the stall region without serious deterioration of over-all performance until a stall-limit line was reached.

The rotating-stall characteristics are summarized in table II. From radial surveys, it was determined that the rotating stall extended over the complete blade span for all speeds and weight flows tested. In

addition, the rotating stall took the form of a single zone rotating at 60 to 70 percent of the rotor speed. The number of stall zones did not increase with increasing back pressure (decreasing weight flow).

Some direct comparisons between the Langley transducer and the hot-wire traces (described in appendix C) are shown in figure 10. The stall data given in table II were obtained from photographs of a four-channel oscilloscope that had signal inputs from two Langley transducers, and two hot-wire anemometers (figs. 10(a) and (b)) or two Langley transducers, a hot-wire anemometer and a 60-cycle signal (figs. 10(c) and (d)). The distance between pulses, or frequency, is the same for both instruments. Phase differences shown are largely results of uneven circumferential spacing of the probes, although the length of lead to a Langley pickup does introduce some phase lag. As a result, the probes for the two Langley pickups located at known circumferential angles should be identical when the number of zones is to be determined from the phase shift.

CONCLUDING REMARKS

The tip section was purposely loaded beyond the prudent diffusion-factor limits. The tip contour and, hence, loading could then be altered stepwise until the highest loading compatible with an acceptable tip loss factor was determined. As indicated by a comparison of the tip pressure ratio and enthalpy rise, the test results from this initial tip configuration indicated severe tip losses. It is not possible from the data now available to determine conclusively whether these losses result solely from the excessive diffusion factor, or whether there are independent effects of Mach number or static-pressure rise on the various surfaces.

Actually, the measured tip losses at design speed even exceed those high losses indicated from the available diffusion-factor - loss-factor relations. This observation suggests that an effort might be made to find a new tip loading parameter that would be more appropriate to the current tip loading and Mach number levels. When such a loading form (including all the factors contributing to the losses) is found, the problem of maximizing the tip work level within the allowable loss limit will be simplified.

Any new tip loading parameter would depend heavily on the blade surface peak velocity. However, the computation of the maximum blade surface velocity depends, in turn, on knowledge of the three-dimensional-annulus configuration. Consequently, any designs that incorporate high weight flow and high Mach numbers should have their streamlines in the radial-axial plane determined by (at least) an approximate three-dimensional design procedure throughout the entire flow field, if good efficiency and accurate design control are to be achieved. Moreover, in this manner, some measure of control may be exercised over the blade surface velocity gradients, and a compatible radial distribution of static pressure might be maintained.

[redacted]

The approximate annular-inlet design procedure was felt to be a step in the direction of ideal design control of the distribution of absolute inlet velocity in spite of the discrepancies between the design and experimental profiles. Inability to measure the exact radial distribution of static pressure at the axial position of the leading edge of the rotor blade hub section (the axial position of the computed design values) and the possibility of nonuniform upstream flow each contributed an indeterminate portion to the observed discrepancy. The existing differences in average absolute Mach number level were discovered to result entirely from the error in blade-setting angle of +1.75°.

Finally, for the level of blade mean relative velocities of the subject rotor, it appears highly desirable that the weight flow be integrated from blade pressure surface to the suction surface as well as in the radial-axial plane. In this manner, the blade-passage flow capacity based on mean velocity may be checked.

SUMMARY OF RESULTS

Separate tests of a transonic rotor designed both as the first stage of a two-stage counterrotating compressor and as a modifiable high-performance transonic-stage test vehicle indicate the following results:

1. The performance of the first stage suffered from high tip losses, which compromised the over-all efficiency.

2. The prerotation set up for the second stage remained near design despite the fact that losses were greater than anticipated.

3. At design speed, the peak over-all efficiency of 0.87 occurred at a pressure ratio of 2.0 and a specific weight flow of 29.2 pounds per second per square foot. Corrected design values indicated a peak over-all efficiency of 0.92 at a pressure ratio of 2.03 and a specific weight flow of 29.2 pounds per second per square foot.

4. The weight flow at which peak efficiency occurred corresponded closely to the weight flow for design average incidence angle, when the 1.75° error in blade-setting angle was applied.

5. Considered as the first stage of a conventional axial-flow compressor, where stators are required to complete the stage, the best performance was found to be at 80 percent of design speed. At this speed, a pressure ratio of 1.56, rotor adiabatic efficiency of 0.95, and a specific weight flow of 26.6 pounds per second per square foot were obtained.

[redacted]

6. A single full-span rotating-stall zone was found that rotated at approximately 65 percent of actual rotor speed at rotor speed of from 50 to 90 percent of design speed.

Lewis Flight Propulsion Laboratory
National Advisory Committee for Aeronautics
Cleveland, Ohio, March 19, 1956

[redacted]

APPENDIX A

SYMBOLS

A_F	compressor frontal area based on inlet tip diameter, sq ft
c_p	specific heat at constant pressure, Btu/(lb)($^\circ$R)
H	total enthalpy, Btu/lb
j	radial station in grid system
M	Mach number
$\left.\begin{matrix} m \\ n \end{matrix}\right\}$	coefficients, eq. (2)
r	compressor radius, in.
r_c	radius of curvature, in.
S	entropy, Btu/lb
T	total or stagnation temperature, $^\circ$R
t	static or stream temperature, $^\circ$R
U	rotor speed
u	function value
V	velocity, ft/sec
w	weight flow, lb/sec
z	axial distance, in. or ft
β	air angle, angle between air velocity and axial direction, deg
γ	ratio of specific heats
δ	ratio of total pressure to NACA standard sea-level pressure of 2116 lb/sq ft
ε	angle between flow direction and axis in radial-axial plane, deg
η	efficiency

[redacted]

θ ratio of total temperature to NACA standard sea-level temperature of 518.7° R

ρ static air density, slugs/cu ft

σ solidity, ratio of chord to spacing

ω angular velocity, radians/sec

Subscripts:

ad adiabatic

h hub

r radial direction

t tip

z axial direction

θ tangential direction

0 free stream

1 rotor inlet

2 rotor outlet

Superscripts:

— mass-averaged value

' relative to rotor

APPENDIX B

ROTOR-OUTLET DESIGN COMPUTATIONS

In order to complete the first-rotor design on a blade-element basis, it was first necessary to determine the design velocity components along the blade span at the trailing edge. The thermodynamic properties (enthalpy, entropy, and stagnation density) were already fixed as functions of percent weight flow between the reference radius (tip) and the radius in question as described in the ROTOR DESIGN section. From an aerodynamic viewpoint then, the compatible (satisfying tip thermodynamic requirements) tip outlet velocity diagram was specified along with the absolute velocity distribution along the outer casing downstream of the rotor. The problem was then to complete the determination of the velocity magnitude and direction everywhere in the annulus between rotors, which satisfied the specified thermodynamic conditions of the fluid and provided a desirable aerodynamic configuration. The second-rotor inlet velocity distribution and the first-rotor diffusion factor (ref. 4), as well as the velocity changes within the statorless interrotor space, had to be considered. Moreover, the initial slope of the inner wall of the interrotor space should approximate that of the prefixed conical first-rotor hub surface. The solution to this problem required some iteration.

Initial computations with a constant outer radius indicated that, for the prescribed outlet enthalpy and entropy distribution, a large hub surface cone angle resulted. This large angle then led to very large radial velocity components at and near the hub. In order to decrease this hub angle and the corresponding radial velocity component at the first-stage outlet, a decrease in tip radius was specified by the following expression:

$$r_t = 8.000 - 0.0438z^3 + 0.01464z^4 - 0.0013z^5 \qquad (1)$$

Use of this equation resulted in a 0.400-inch reduction in tip radius over the first rotor.

The radial component of the equations of motion, along with the continuity equation (eqs. (13) and (14) of ref. 12), were used in the interrotor region for determination of the flow conditions. Omitting the nonsignificant blade force terms and assuming a nonviscous fluid, the resulting equation of motion applies in the interrotor annulus:

$$\frac{\partial H}{\partial r} = t\frac{\partial S}{\partial r} + \frac{V_\theta}{r}\frac{\partial (rV_\theta)}{\partial r} + V_z\frac{\partial V_z}{\partial r} - V_z\frac{\partial V_r}{\partial z} \qquad (B1)$$

while the continuity equation is given as

$$\frac{1}{r}\frac{\partial(rV_r)}{\partial r} + \frac{\partial V_z}{\partial z} + \frac{1}{\gamma - 1}\left(V_r \frac{\partial \ln t}{\partial r} + V_r \frac{\partial \ln t}{\partial r}\right) - V_r \frac{\partial\left(\frac{S}{R}\right)}{\partial r} - V_z \frac{\partial\left(\frac{S}{R}\right)}{\partial z} = 0 \tag{B2}$$

(All symbols are defined in appendix A.)

The solution to these equations was carried out along grid lines of constant radius (fig. 1) except at the tip, where the radius of the tip contour still varied according to equation (1). Equations (B1) and (B2) may also be solved along the tip contour in a manner similar to that along grid lines with the aid of relations between the total and partial derivatives of the variables.

Three axial stations (z = 0, 0.05, and 0.10 ft after rotor hub exit) were selected, through which radial lines were drawn. Axial grid lines were then drawn at constant radii (r = 0.607, 0.577, 0.547, 0.517, 0.487, 0.457, 0.427, and 0.397, see fig. 1). The values of V_z were assumed along the tip at the specified z-positions, and V_θ was computed from the expression

$$V_\theta = \frac{\Delta H}{\omega r}$$

at the rotor outlet.

Downstream values (in the interrotor space) of $V_\theta = V_{\theta,2}(r_2/r)$. At any point, $V_r = V_z \tan \varepsilon$ where $\tan \varepsilon$ is given by the derivative of the tip contour expression. The total temperature T_2 may be expressed as follows:

$$T_2 = \frac{c_p T_1 + \Delta H}{c_p} \tag{B3}$$

For the final calculation, a constant enthalpy and, hence, constant T_2 were used along the blade span.

Then, with all velocity components known and the stagnation density given at the tip, the stream temperature, the velocity of sound, the Mach number, and the stream density were found. The weight flow was approximated through the tip incremental annulus, using tip conditions and mean

[redacted]

annular radius in the following expression:

$$\Delta w_j^{j+1} = 2\pi r \Delta r (\rho V_z)_j \qquad (B4)$$

The accumulated mass between the tip $j = 0$ and any local radial position j was $\sum_0^j \Delta w$.

The entropy, enthalpy, and total density were then found at $(j + 1)$ as a function of percent weight flow. All derivatives with respect to r were approximated by dividing the small incremental changes from j to $(j + 1)$ by $r_j - r_{j+1}$. In order to obtain the partial changes with respect to z on a constant-radius grid line, the following three-point-differentiation formula was used:

$$\frac{\partial u}{\partial z} = \frac{u_{2c} + u_{2a} - 2u_{2b}}{0.0025} z + 40u_{2b} - 30u_{2a} - 10u_{2c} \qquad (B5)$$

The grid spacing used is indicated in figure 1. The subscripts 2a, 2b, and 2c indicate the first, second, and third stations, respectively, downstream of the rotor outlet, whereas u represents any function known at the designated points. Hence, any quantity for which values are known on the horizontal grid line could be substituted into (B5) to obtain its partial derivative with respect to z at that point. The equations (B1) and (B2) were solved to give ultimately $\partial V_r/\partial r$ from which V_r could be found on the adjacent horizontal grid line. This process was continued along r until 100-percent weight flow was obtained. The locus of the 100-percent-weight-flow streamline, which identifies the hub contour, was then found by radial interpolation between the appropriate grid points. Streamlines through the rotor were then approximated by straight lines joining points at the blade inlet to the points of corresponding percent weight flow at blade outlet.

The possibility existed that either the hub contour, the radial variation of conditions at the end of the interrotor space, or the velocity changes along any streamlines across the first-stage rotor would not meet the design requirements. In this event, the designer could then alter the assumed tip axial velocity distribution, the tip wall contour between rotors, and/or the distribution of any of the thermodynamic properties across the first-stage rotor and continue the computations until a satisfactory configuration is reached. In practice, the tip axial velocity distribution usually has sufficient effect on the computational results so that no other terms need be altered. If, however, the tip wall V_z distribution cannot be changed sufficiently to lead to the

desired results, change in either the enthalpy input (which, of course, means a change in pressure ratio for no change in loss distribution) or the tip wall contour affords powerful means of altering the final flow configuration.

[redacted]

APPENDIX C

ROTATING-STALL APPARATUS

The type of equipment employed at the time of these tests for determining rotating-stall characteristics consisted of a 0.0002-inch hot-wire anemometer with an Ossofsky amplifier unit, variable electronic filters, various bridges, and an oscilloscope (see ref. 13). The wires were very fragile and did not last long under stall conditions. For much of the current test work, it is only necessary to determine whether rotating stall exists and, if so, the frequency and radial extent. For this use, a rugged pickup with long life would be preferred.

The frequency response of a Langley transducer (ref. 14) is adequate for the frequency range of rotating-stall pulses if the pressure leads are short enough to prevent attenuation of the signal. In order to make radial surveys, however, some length of lead is inevitable. The arrangement shown in figure 11 was devised to use a transducer with the maximum sensitivity without amplification. The probe shown has four pressure orifices; the two side tubes are for the automatic angle device to keep the probe pointed into the stream. The bottom tube (a pitot tube) is led off to an acoustic trap (4 ft of 0.030- by 0.003-in. wall tubing; volume, approx. 1 cu in.) to one side of the Langley pickup. This provides a steady pressure that is the same as the average total pressure in the fluctuating stream. The top tube goes directly to the pressure pickup with as short a lead as possible. Thus, the pressure difference on the diaphragm of the pickup is only the difference due to the unsteady flow; a sensitive instrument ($\pm 1/2$ lb/sq in.) may be used. In addition to the probe, pickup, and acoustic trap, a simple adjusting bridge, an oscillator, and an oscilloscope are required. (The signal was superimposed on a 10,000-cycle carrier wave.) This equipment is actually much simpler and more reliable than the hot-wire equipment, though its use for quantitative data is limited. For these tests, a four-channel oscilloscope was used to allow direct comparison of a hot-wire anemometer and a Langley transducer and to carry a 60-cycle wave for reference purposes.

REFERENCES

1. Wilcox, Ward W.: An Analysis of the Potentialities of a Two-Stage Counterrotating Supersonic Compressor. NACA RM E52E01, 1952.

2. Wilcox, Ward W.: Investigation of Impulse-Type Supersonic Compressor with Hub-Tip Ratio of 0.6 and Turning to Axial Direction. I - Performance of Rotor Alone. NACA RM E54B25, 1954.

3. Stewart, Warner L., Schum, Harold J., and Whitney, Warren J.: Investigation of Turbines for Driving Supersonic Compressors. I - Design and Performance of First Configuration. NACA RM E52C25, 1952.

4. Lieblein, Seymour, Schwenk, Francis C., and Broderick, Robert L.: Diffusion Factor for Estimating Losses and Limiting Blade Loadings in Axial-Flow-Compressor Blade Elements. NACA RM E53D01, 1953.

5. Lieblein, Seymour, Lewis, George W., Jr., and Sandercock, Donald M.: Experimental Investigation of an Axial-Flow Compressor Inlet Stage Operating at Transonic Relative Inlet Mach Numbers. I - Over-All Performance of Stage with Transonic Rotor and Subsonic Stators up to the Rotor Relative Inlet Mach Number of 1.1. NACA RM E52A24, 1952.

6. Serovy, George K., Robbins, William H., and Glaser, Frederick W.: Experimental Investigation of a 0.4 Hub-Tip Diameter Ratio Axial-Flow Compressor Inlet Stage at Transonic Inlet Relative Mach Numbers. I - Rotor Design and Over-All Performance from 60 to 100 Percent of Design. NACA RM E53I11, 1953.

7. Schwenk, Francis C., Lieblein, Seymour, and Lewis, George W., Jr.: Experimental Investigation of an Axial-Flow Compressor Inlet Stage Operating at Transonic Relative Inlet Mach Numbers. III - Blade-Row Performance of Stage with Transonic Rotor and Subsonic Stator at Corrected Tip Speeds of 800 and 1000 Feet Per Second. NACA RM E53G17, 1953.

8. Klapproth, John F., Jacklitch, John J., Jr., and Tysl, Edward R.: Design and Performance of a 1400-Foot-Per-Second Tip-Speed Supersonic Compressor Rotor. NACA RM E55A27, 1955.

9. Wilcox, Ward W.: Investigation of Impulse-Type Supersonic Compressor with Hub-Tip Ratio of 0.6 and Turbine to Axial Direction. II - Stage Performance with Three Different Sets of Stators. NACA RM E55F28, 1955.

10. Stewart, Warner L.: Investigation of Rotating Components of Counter-rotating Two-Spool Engines. I - Analytical Investigation of Off-Design Performance of Turbine Component Designed with and without Outer-Turbine Stator. NACA RM E54J13, 1955.

11. Carter, A. D. S.: The Low-Speed Performance of Related Airfoils in Cascade. Rep. No. R.55, British N.G.T.E., Sept. 1949.

12. Wu, Chung-Hua, and Wolfenstein, Lincoln: Application of Radial-Equilibrium Condition to Axial-Flow Compressor and Turbine Design. NACA Rep. 955, 1950.

13. Ossofsky, Eli: Constant Temperature Operation of the Hot-Wire Anemometer at High Frequency. Rev. Sci. Instr., vol. 19, no. 12, Dec. 1948, pp. 881-889.

14. Patterson, John L.: A Miniature Electrical Pressure Gage Utilizing a Stretched Flat Diaphragm. NACA TN 2659, 1952.

[redacted]

TABLE I. - ROTOR DESIGN CONFIGURATION

[Incidence angle, 5°.]

Stream surface, percent mass from tip	Stream surface radius, in.		Flow angle, deg		Solidity, σ
	Inlet, r_1	Outlet, r_2	Inlet, ε_1	Outlet, ε_2	
0	7.97	7.63	63.94	44.20	1.234
20	7.33	7.12	60.65	29.81	1.332
40	6.66	6.67	57.20	21.99	1.413
60	5.92	6.18	53.53	13.53	1.591
80	5.06	5.61	49.57	1.38	1.804
100	4.00	4.89	45.49	-16.65	2.164

TABLE II. - STALL CHARACTERISTICS

[One stall zone; root-to-tip stall.]

$\frac{w\sqrt{\theta}}{\delta A_F}$, lb/(sec)(sq ft)	Rotor speed		Stall frequency, cps	Stall speed, percent rotor speed
	% design	rps		
13.15	50	153.5	102	67.5
11.75	50	153.9	102	67.5
10.28	50	154.0	102	65.6
12.53	50	153.8	100	65.0
16.42	60	184.0	123	70.7 or 67
14.76	60	184.0	118	63.6
13.14	60	184.0	123	65.7
19.21	70	214.0	148	69.2
22.11	80	245.5	160	65.4
24.64	90	276.0	169	61.2

[redacted]

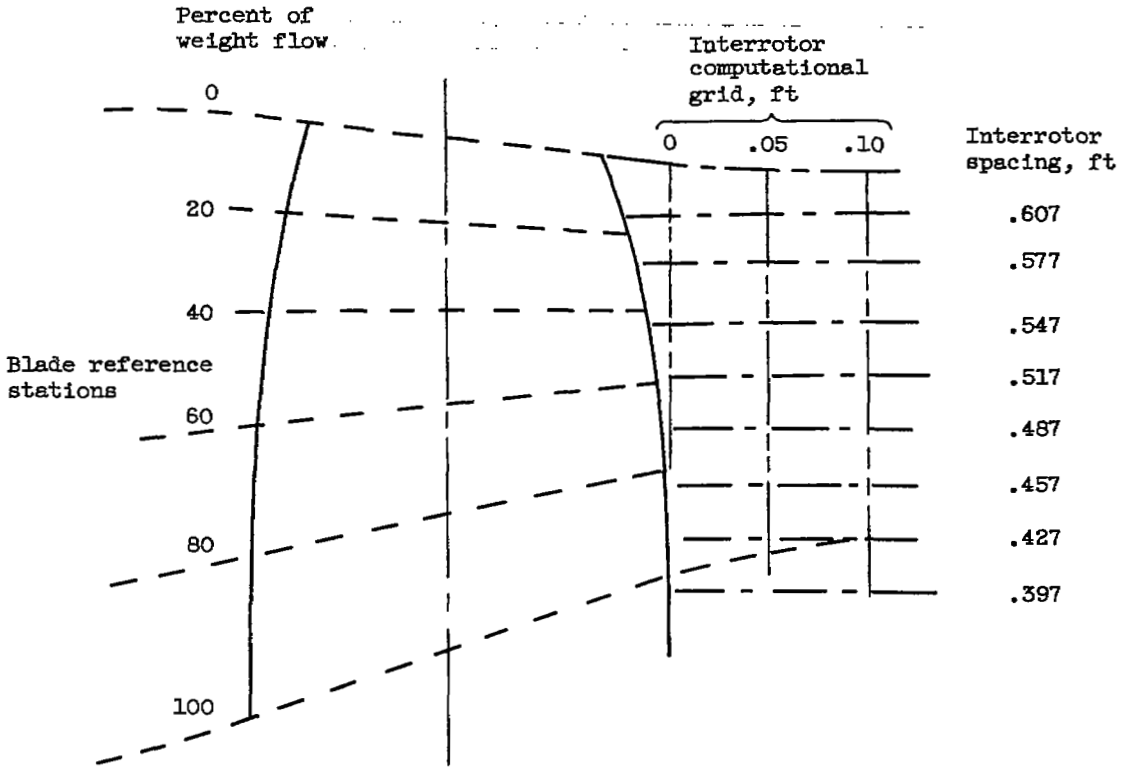

Figure 1. - First-stage rotor computational layout in radial-axial plane.

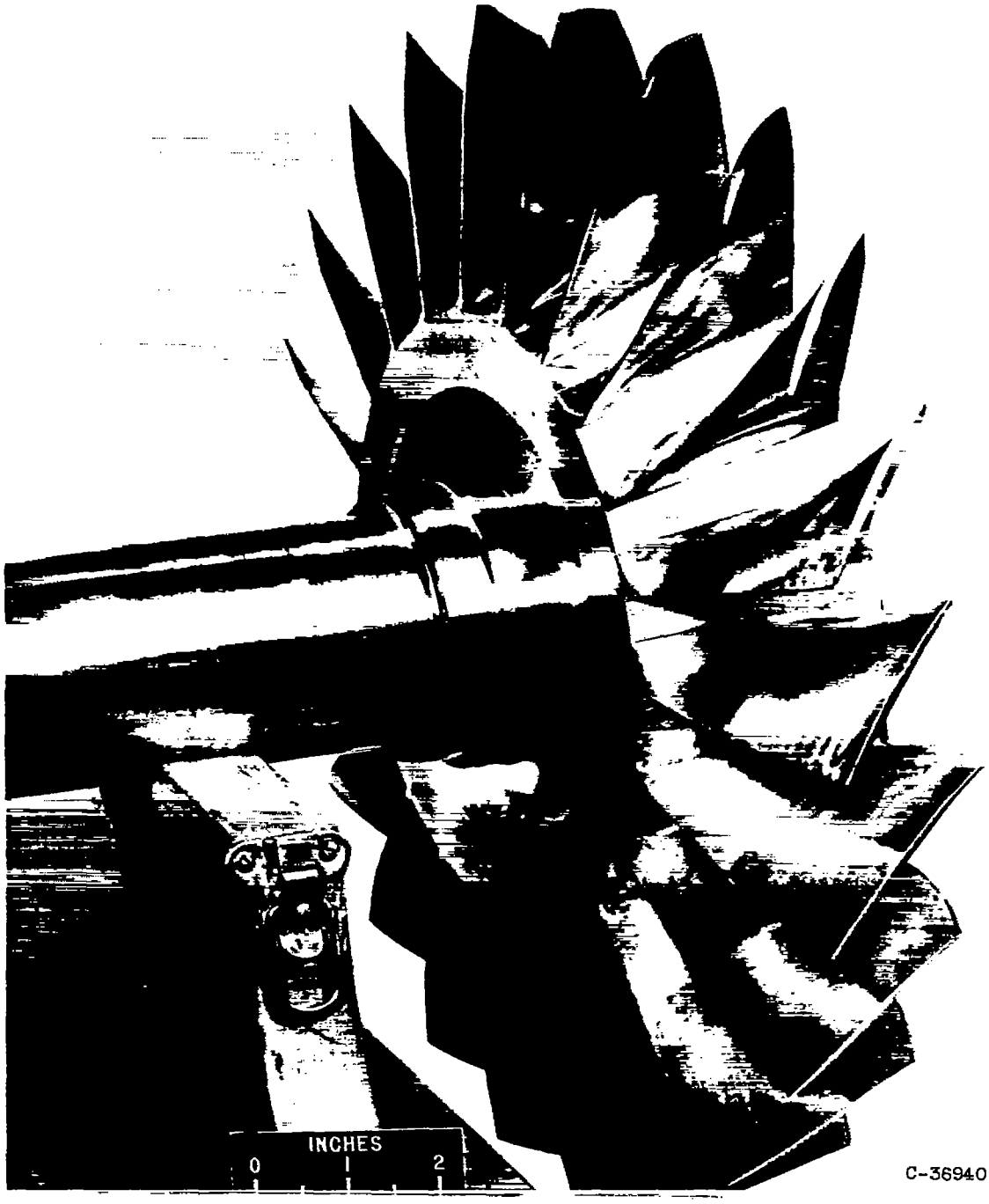

(a) Photograph of rotor.

Figure 2. - First-stage rotor of counterrotating supersonic compressor.

[redacted]

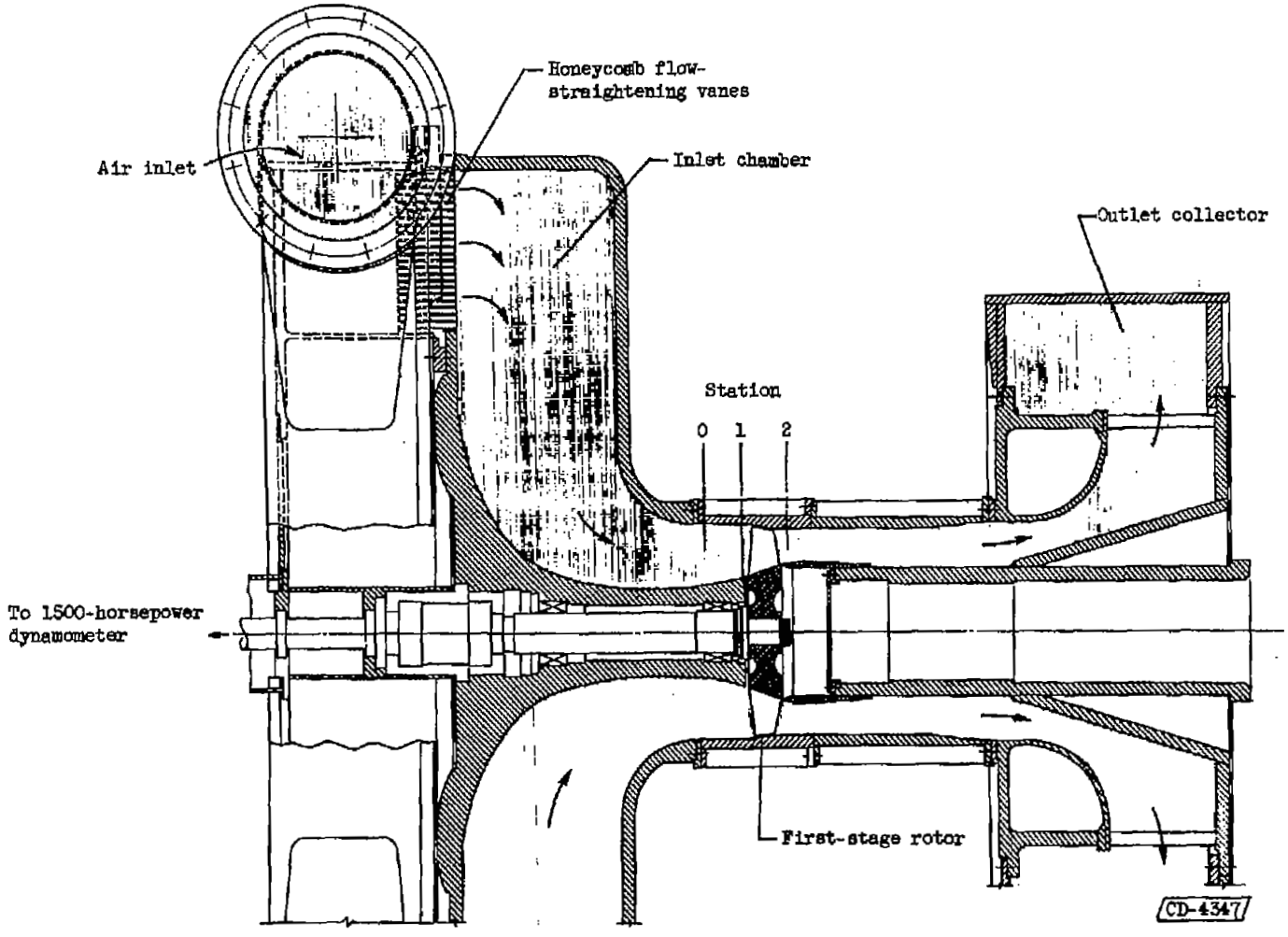

(b) Sketch of rotor installation in test rig.

Figure 2. - Concluded. First-stage rotor of counterrotating supersonic compressor.

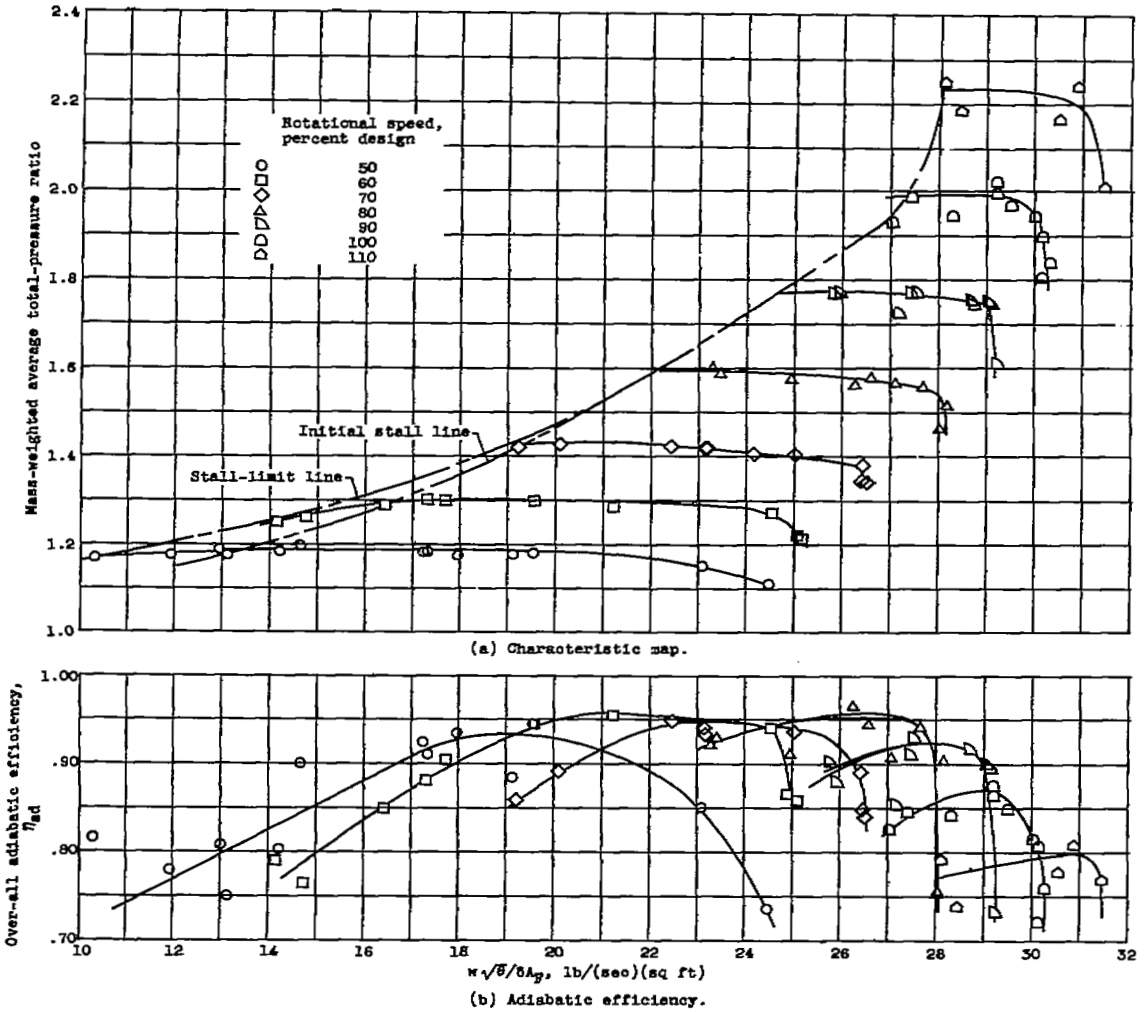

Figure 3. - Over-all performance of first-stage rotor of counterrotating compressor.

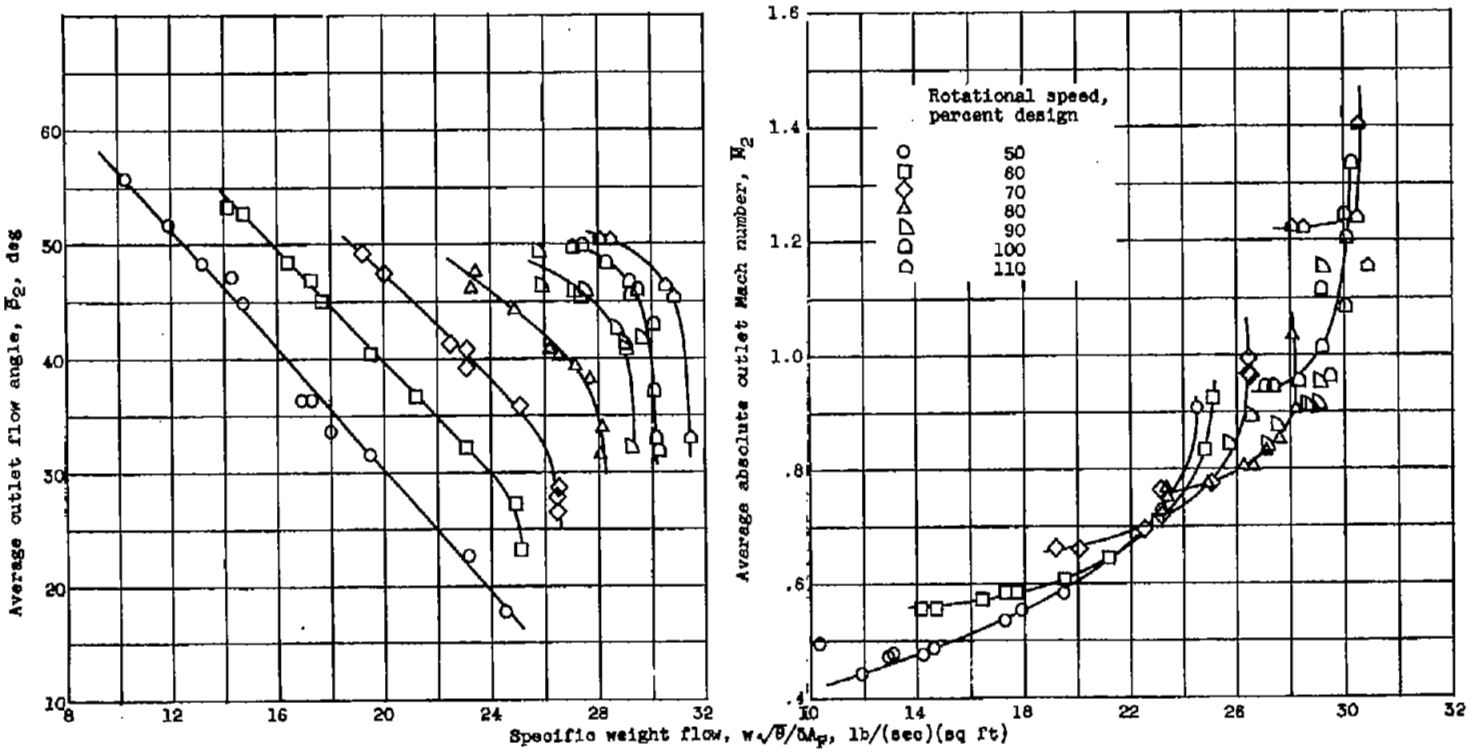

(c) Mass-weighted average outlet flow angle.

(d) Mass-weighted average outlet absolute Mach number.

Figure 5. - Concluded. Over-all performance of first-stage rotor of counterrotating compressor.

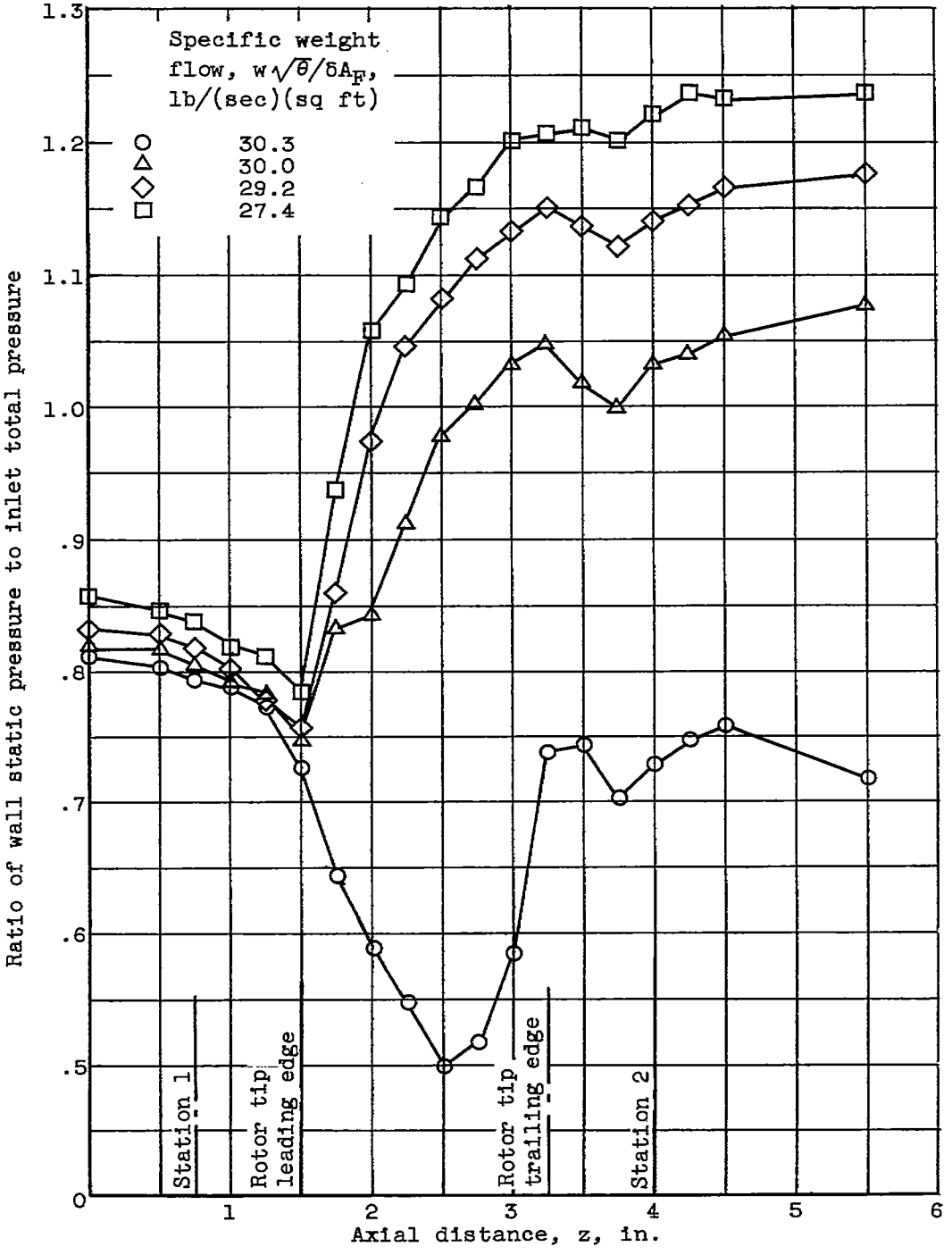

Figure 4. - Static-pressure distribution along outer wall.

[redacted]

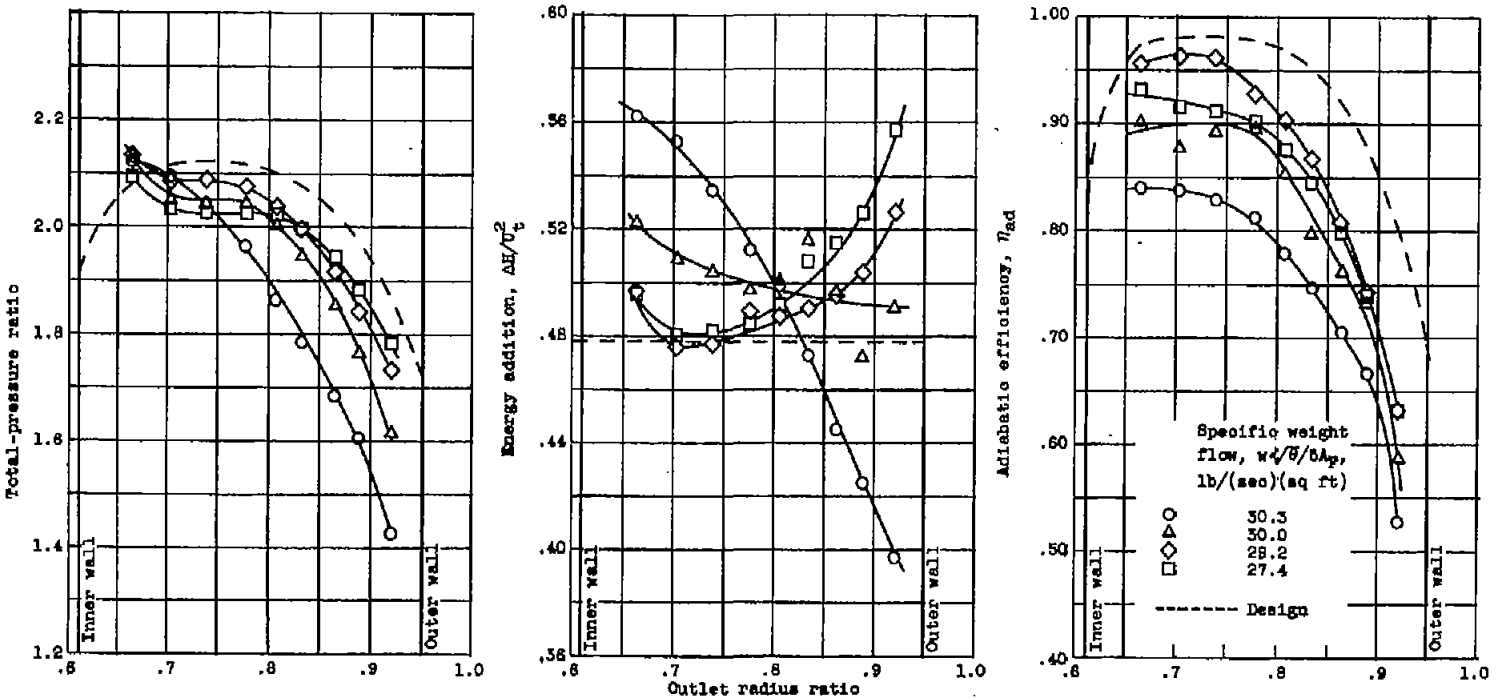

(a) Total-pressure ratio. (b) Energy addition. (c) Adiabatic efficiency.

Figure 5. - Radial variation of pressure ratio, energy addition, and adiabatic efficiency for first-stage rotor of counterrotating compressor at design speed of 1260 feet per second.

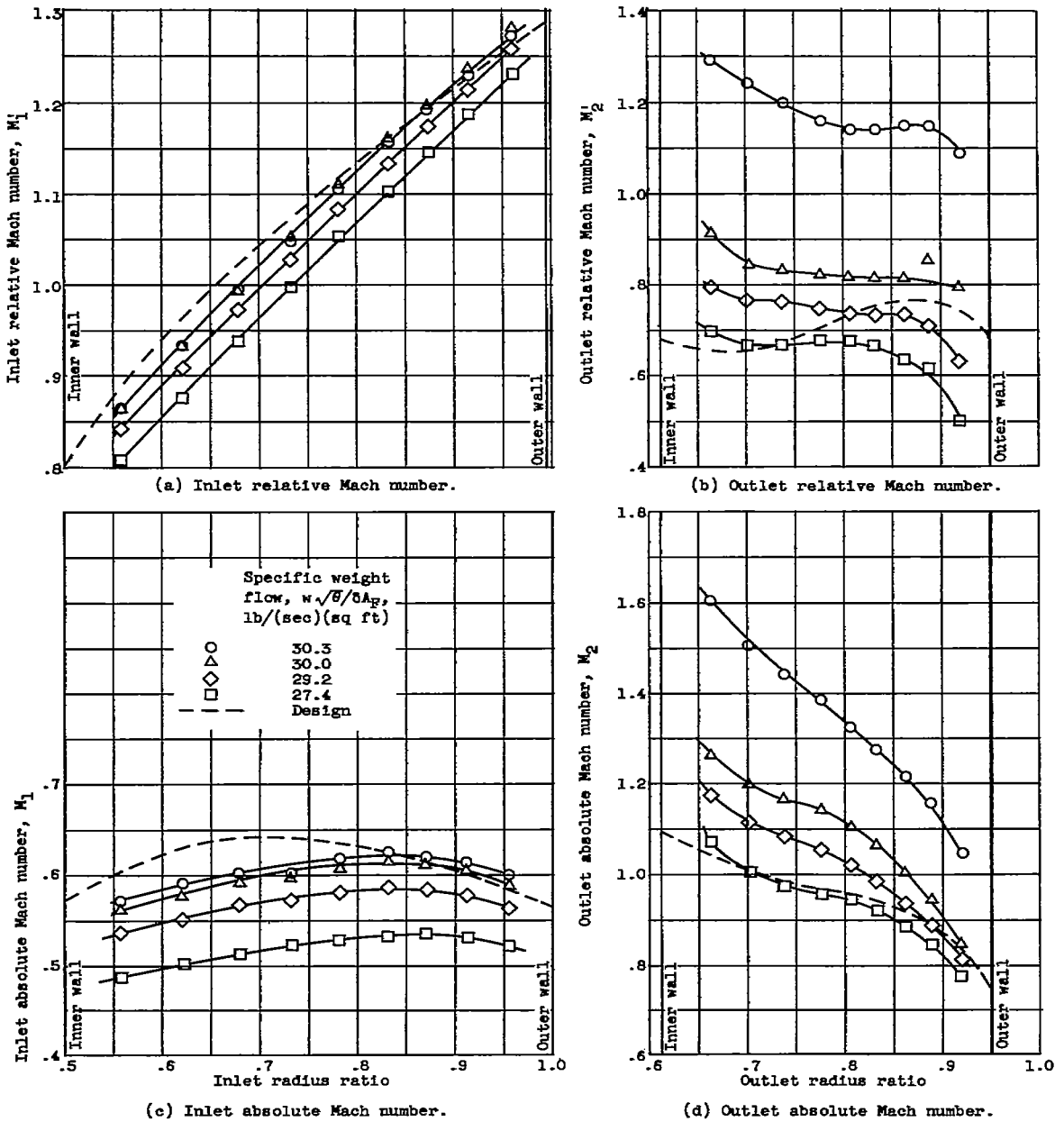

Figure 6. - Radial variations of Mach numbers for first-stage rotor of counterrotating compressor at design speed of 1260 feet per second.

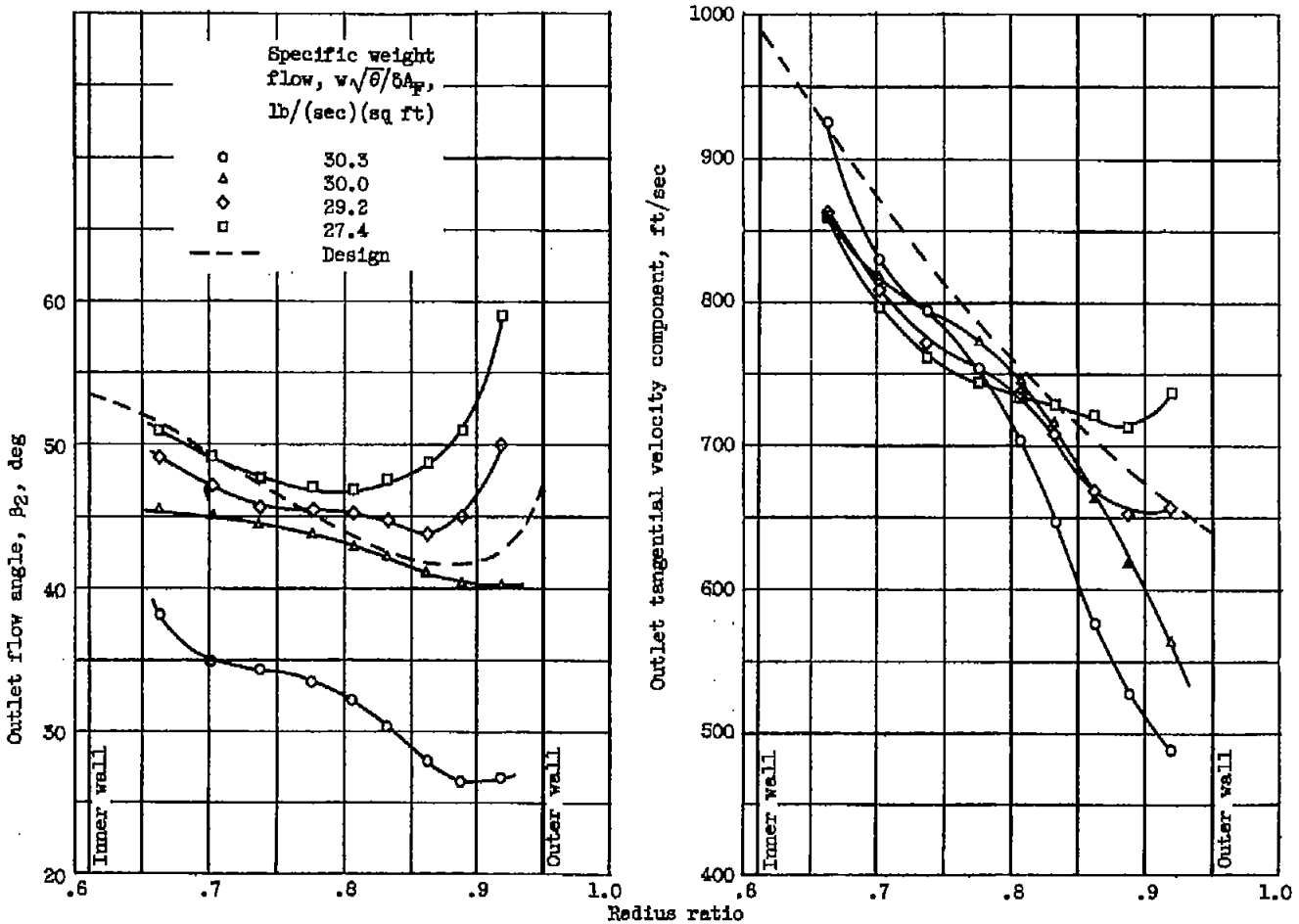

(a) Outlet flow angle.

(b) Outlet tangential velocity.

Figure 7. - Radial variation of outlet flow angle and tangential velocity component for first-stage rotor of counterrotating compressor at design speed of 1260 feet per second.

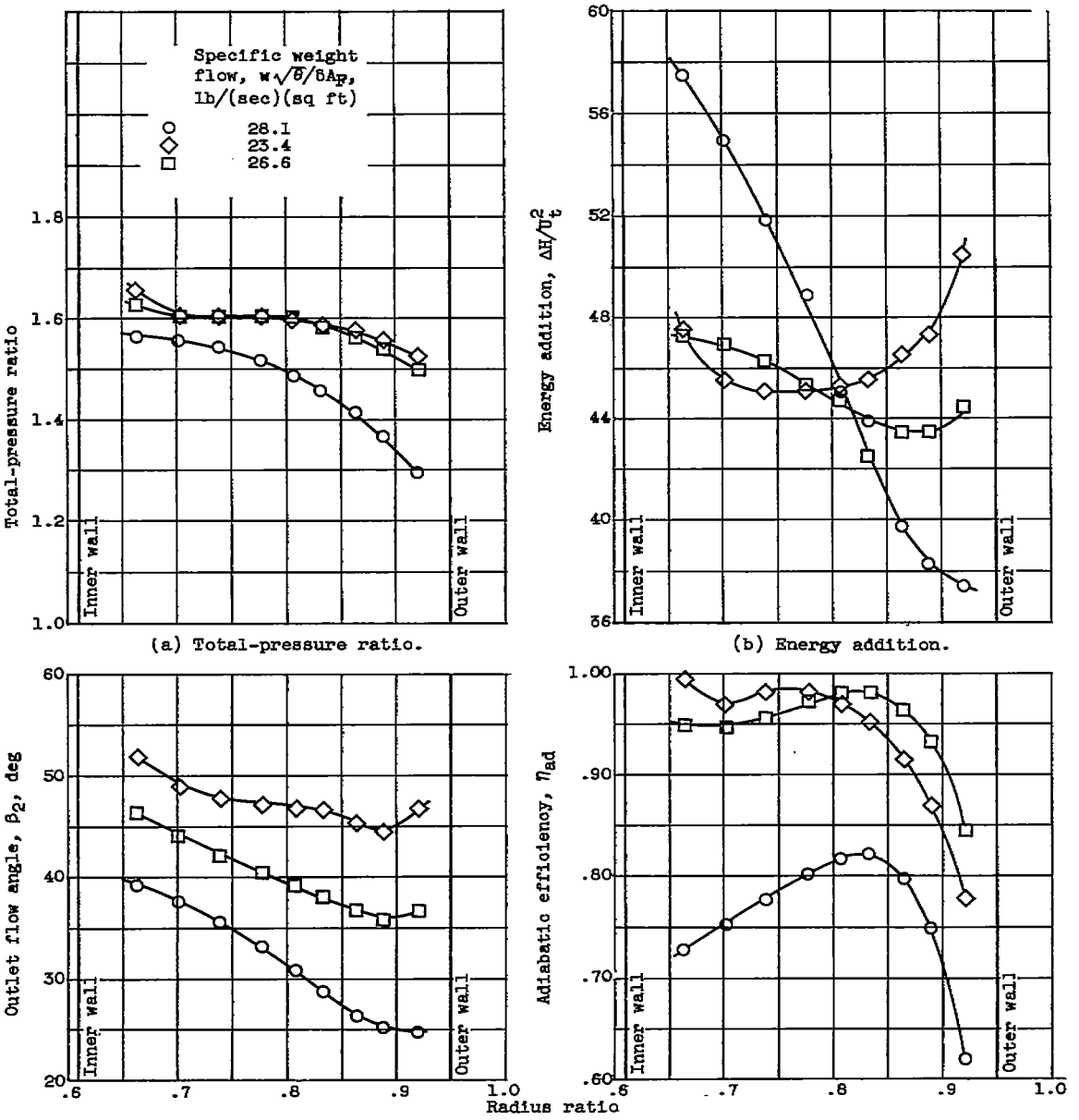

(a) Total-pressure ratio.

(b) Energy addition.

(c) Outlet flow angle.

(d) Adiabatic efficiency.

Figure 8. - Radial variation of performance parameters at 80 percent of design speed.

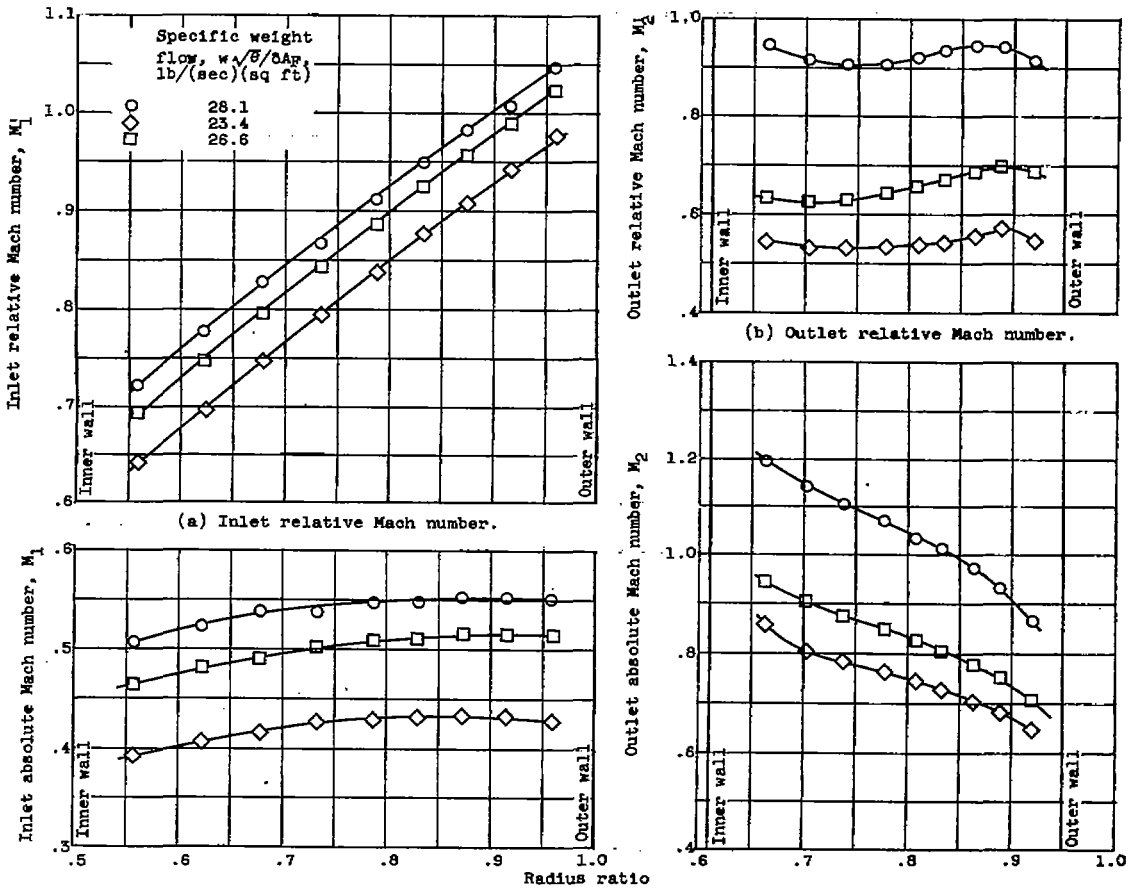

(a) Inlet relative Mach number.

(b) Outlet relative Mach number.

(c) Inlet absolute Mach number.

(d) Outlet absolute Mach number.

Figure 9. - Radial variation of Mach numbers at 80 percent of design speed.

[redacted]

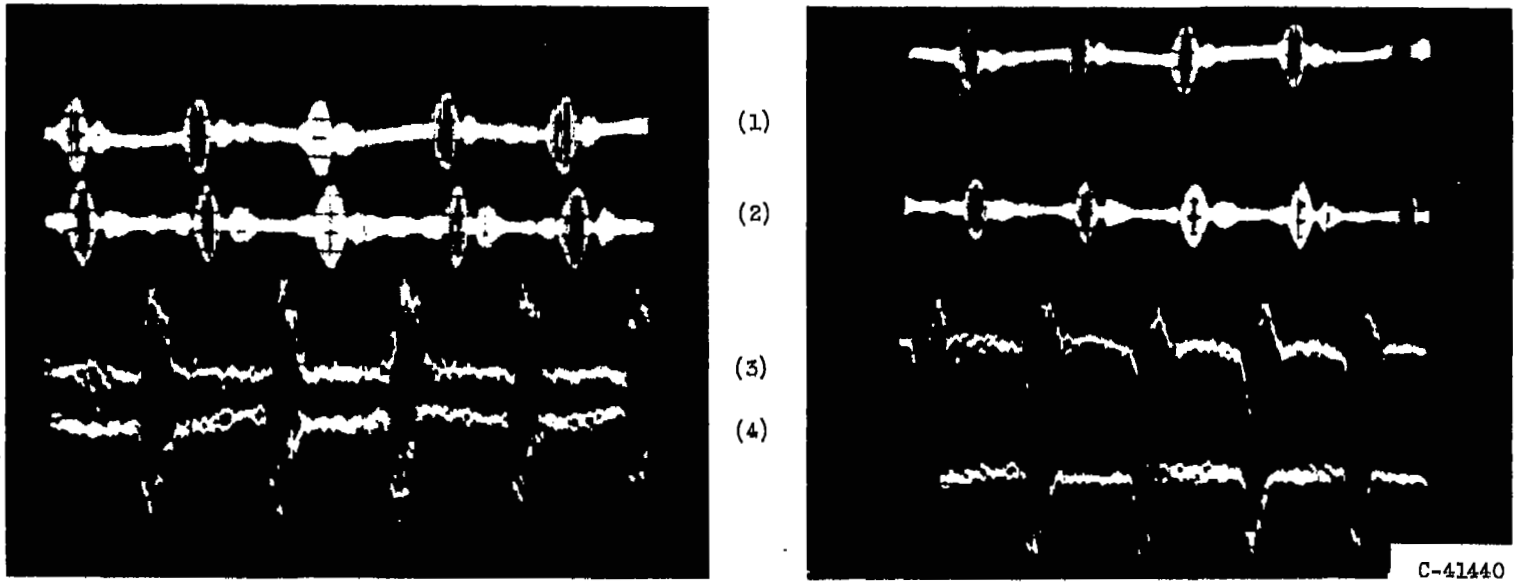

(a) Speed, 50-percent design; stall frequency, 100 cps; radial position 2; specific weight flow, 12.53 pounds per second per square foot.

(b) Speed, 50-percent design; stall frequency, 100 cps; radial position 7; specific weight flow, 12.53 pounds per second per square foot.

(1) Langley probe in front.
(2) Langley probe in rear.
(3) Hot wire in front.
(4) Hot wire in rear.

Figure 10. - Comparison of hot-wire-anemometer and Langley pickup traces.

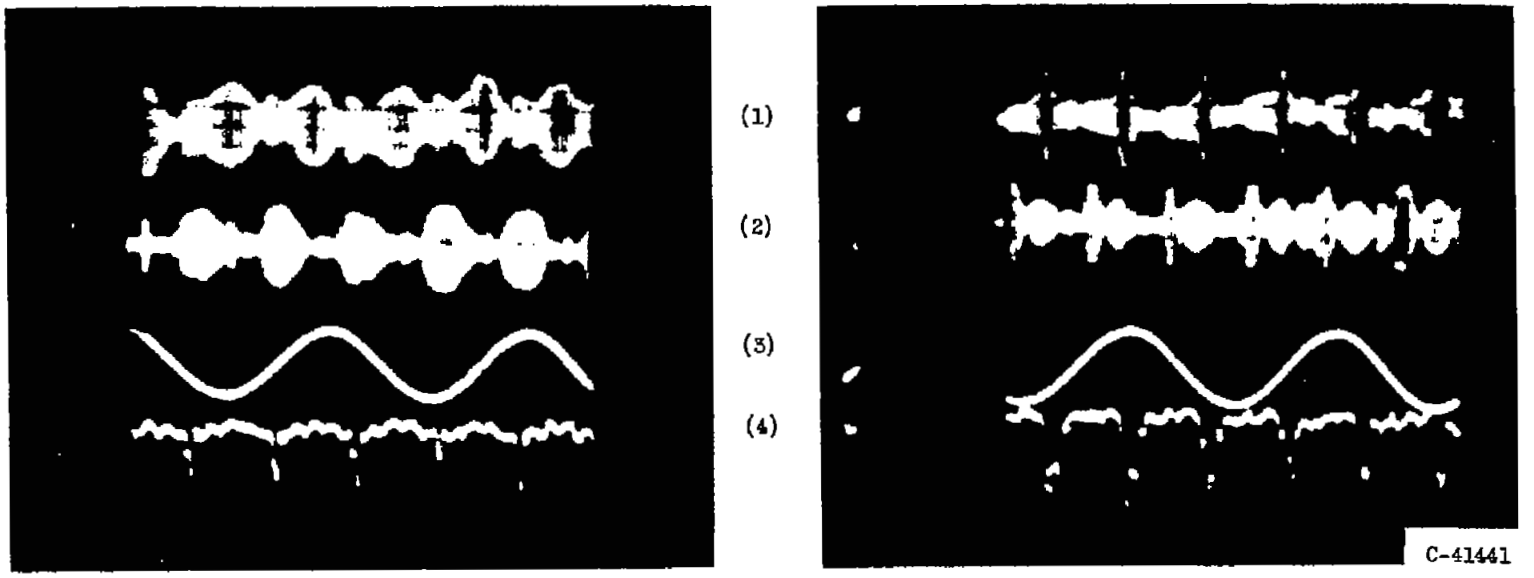

(c) Speed, 70-percent design; stall frequency, 148 cps; radial position 8; specific weight flow, 19.21 pounds per second per square foot.

(d) Speed, 80-percent design; stall frequency, 160 cps; radial position 2; specific weight flow, 22.11 pounds per second per square foot.

(1) Langley probe behind rotor.
(2) Langley probe behind rotor.
(3) 60-Cycle reference.
(4) Hot wire behind rotor.

Figure 10. - Concluded. Comparison of hot-wire-anemometer and Langley pickup traces.

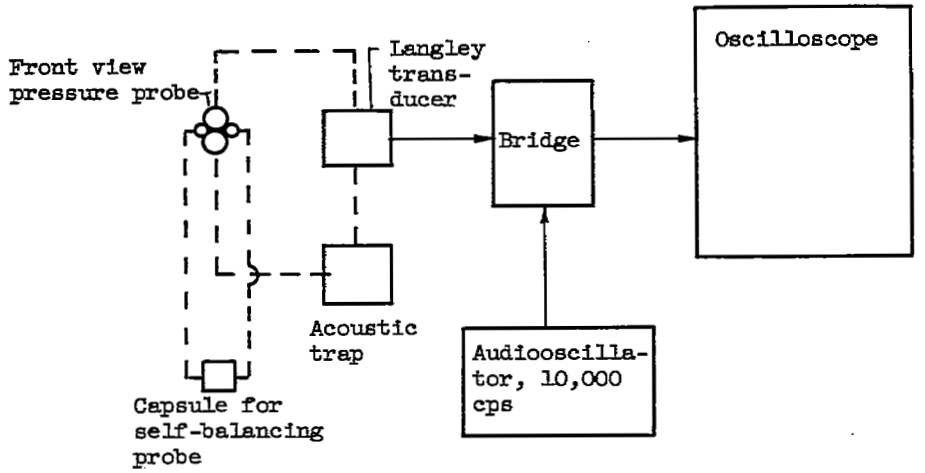

(a) Hookup of Langley transducer as rotating-stall detector.

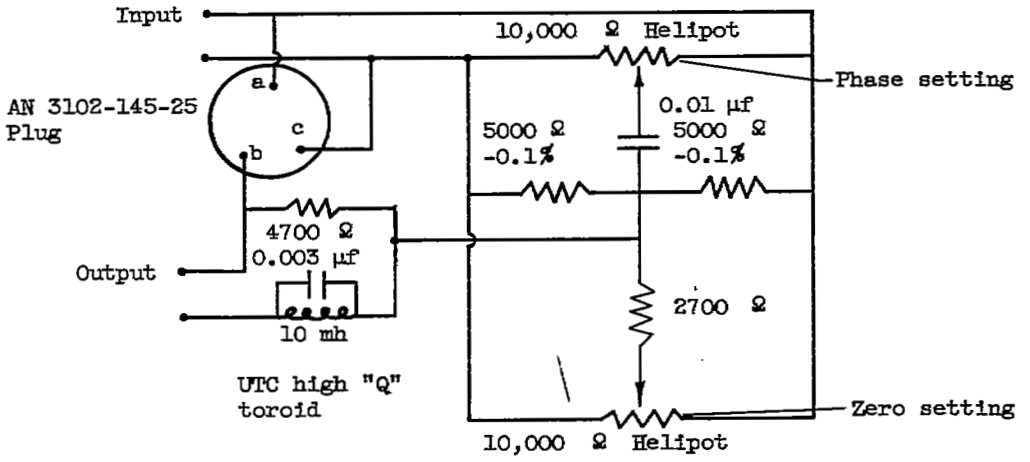

(b) Bridge circuit.

Figure 11. - Langley transducer details.

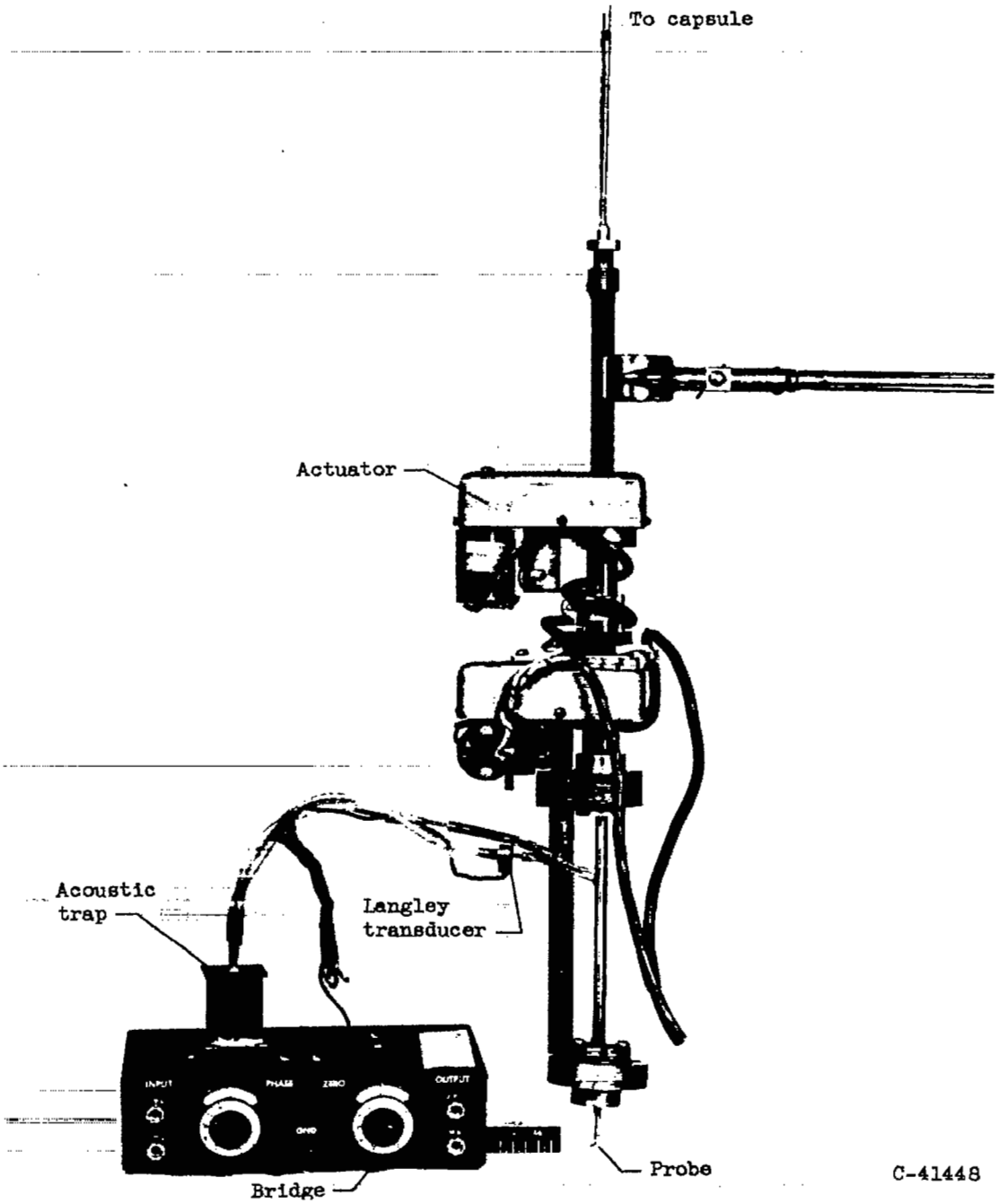

(c) Probe and apparatus for rotating-stall detection and evaluation.

Figure 11. - Concluded. Langley transducer details.